

NEURAL NETWORKS FOR IMPROVED DARK MATTER DETECTION:
ADVANCES IN SNOLAB SUPERCDMS DETECTOR RESOLUTION

A PHY479 Undergraduate Research Project

by

Arsalan Khan
Student Number: 1007065925

Supervised by Professor Pekka K. Sinervo
Department of Physics

Neural Networks for Improved Dark Matter Detection: Advances in SNOLAB
SuperCDMS Detector Resolution

Arsalan Khan
Bachelor of Science

Department of Physics
University of Toronto
2024

Abstract

Dark matter research represents a fundamental quest to unravel the mysteries of the universe's composition and evolution. The SNOLAB SuperCDMS experiment, plays a pivotal role in this pursuit by seeking to maximize sensitivity to low-mass dark matter particles. However, inherent limitations in position and energy resolution within the SuperCDMS detectors pose significant challenges in accurately identifying and characterizing particle interactions. This project explores novel approaches to enhance the resolution and accuracy of the detectors, focusing on the integration of advanced simulation techniques and machine learning methodologies. Through experimentation with datasets generated via FullDMC and FastDMC simulations, various neural network architectures are explored and optimized. Results demonstrate promising improvements in predicting the positions and energies of energy depositions within the detectors. Moreover, comparisons between datasets from different simulation methods provide critical insights into the strengths and limitations of each approach. Ultimately, these advancements will bolster the goals of the SNOLAB SuperCDMS collaboration by enhancing the experiment's sensitivity and precision in detecting elusive dark matter particles.

Acknowledgements

I extend my heartfelt gratitude to Professor Pekka K. Sinervo for his invaluable guidance and for entrusting me with the opportunity to contribute to his research group. His mentorship and dedication to teaching have been instrumental in shaping my understanding and skills in this field. I am deeply grateful to Dr. Madeleine Zurowski and Warren Perry for their unwavering support and prompt responses to my inquiries, which have been immensely beneficial throughout this journey.

I am indebted to Janice Qin, my collaborative partner in this project, for her steadfast companionship and mutual assistance during challenging times. Together, we navigated obstacles and emerged stronger, fostering a collaborative spirit that enriched our work. Additionally, I express my appreciation to Aditi Pradeep for generously sharing insights from her pioneering work, which served as a catalyst for our continued research endeavors.

Lastly, I extend my thanks to the entire team for their understanding and flexibility in accommodating my busy schedule, ensuring productive collaboration and meaningful contributions to our collective goals.

Contents

1	Background	1
1.1	The SuperCDMS Collaboration	1
1.2	SuperCDMS Detectors	2
1.2.1	iZIP Detectors	2
1.2.2	HV Detectors	4
1.2.3	Detector Sensitivity	4
1.3	SuperCDMS Structure	6
1.4	Simulation Techniques	6
1.5	A Brief Overview of Neural Networks	8
1.6	Neural Networks in SuperCDMS	8
2	Previous Work & Motivation	10
3	Experimental Trials	13
3.1	Initial Simulations	13
3.2	Recreating PCA	13
3.3	FullDMC NxM Data & First Trials	16
3.3.1	Data	16
3.3.2	Feedforward Neural Network Exploration & Optimization . . .	16
3.3.3	Discussion	16
3.4	Exploring 1DOF Data	17
3.4.1	Motivation for Investigating Signal Delays	17
3.4.2	Results & Discussion	18
3.5	Exploring FastDMC Data	19
3.5.1	Data	19
3.5.2	Results & Discussion	19
4	Next Steps	24

List of Figures

1.1	The SuperCDMS SNOLAB detectors, from [2]. "SuperCDMS SNO-LAB detectors. (Left) iZIP. (Right) HV. (Top) Prototype detectors in their housings. (Bottom) Channel layout. The iZIP detector has six phonon channels on each side, arranged as an inner core surrounded by four wedge-shaped channels and one outer ring. Each channel contains hundreds of lithographically defined superconducting sensors. An "outer" ionization channel shares the same area and is interleaved with the outermost phonon ring, and an "inner" ionization channel is interleaved with the remaining phonon channels. The wedge channels on the bottom surface are rotated by 45° with respect to those on the top. The HV detector has six phonon channels on each side: an inner core surrounded by three wedge-shaped channels and two outer rings designed to reject events near the edge. The wedge channels on the bottom surface are rotated by 60° with respect to those on the top." .	3
1.2	Exclusion sensitivity of SNOLAB SuperCDMS detectors using "goal" performance and background levels, from TDR [1]. The vertical axis is the spin-independent dark matter-nucleon cross section, and the horizontal axis is the dark matter particle mass.	5
1.3	SNOLAB SuperCDMS apparatus from [2].	6
1.4	SNOLAB SuperCDMS simulation pipeline from [17].	7
2.1	Aditi Pradeep's neural network training results, compared to linear fit, training on NxM phonon amplitudes and predicting X, Y, Z positions from [19].	11
2.2	Aditi Pradeep's boosted decision tree training results, compared to linear fit, training on NxM phonon amplitudes and predicting X, Y, Z positions from [19].	12

3.1	Phonon collection efficiency for 1000 samples from a FullDMC simulation of an iZIP detector. Low efficiency is defined as less than 80% collection efficiency.	14
3.2	Raw phonon pulses at each detector channel from FastDMC of an iZIP detector. The plot titles are the names of the detector channels, the horizontal axis shows time bins of bin width 1600 ns, and the vertical axis shows the amplitudes measured in Amperes.	14
3.3	Principal components found for detector channel PDS1. The horizontal axis shows time bins of bin width 1600 ns, and the vertical axis shows the amplitudes measured in Amperes.	15
3.4	Percent variance of principal components found for each detector channel. Horizontal axis is principal component number.	15
3.5	Training and validation loss of a neural network after training in TensorFlow.	17
3.6	Neural network X, Y, Z predictions from training on four different input parameter cases. Horizontal axis is actual (normalized) values, vertical axis is predicted (normalized) values.	18
3.7	X, Y, Z predictions of neural network trained on FastDMC data. . . .	19
3.8	Energy predictions from neural network trained on FastDMC data. .	20
3.9	1D histograms of X and Y predictions from neural network trained on FastDMC data compared to actual values.	20
3.10	2D histogram of X and Y predictions from neural network trained on FastDMC.	21
3.11	Left: Phonon amplitudes measured by detector channel PCS1 from FastDMC dataset, plotted by Warren Perry. Middle: Inverse of left plot to represent opposite detector face. Right: Overlap of middle and left plots to represent neural network's view of X and Y datapoints. . .	22
3.12	Left: Phonon amplitudes measured by detector channel PCS1 from FullDMC dataset, plotted by Warren Perry. Right: 2D histogram of X and Y predictions from neural network trained on FullDMC. . . .	22

Chapter 1

Background

1.1 The SuperCDMS Collaboration

Astronomical observations show that starts in galaxies in our universe move at such high speed that the mass attributed to them can not possibly hold them together. This leads scientists to believe that something else that we cannot see is at work [3]. Dark matter is a pervasive yet elusive substance that constitutes a substantial portion of the universe’s mass [4]. Weakly interacting massive particles (WIMPs) [5, 6] are a potential dark matter candidate that have been the focus for the majority of direct dark matter searches [7, 8, 9, 10].

The SNOLAB Super Cryogenic Dark Matter Search (SuperCDMS) collaboration is one such experiment addressing the challenge of detecting and identifying dark matter particles, elementary particles that are not predicted by the Standard Model of particle physics. The primary goal is to significantly increase the sensitivity for detecting dark matter particles with masses up to $10 \text{ GeV}/c^2$, exceeding existing capabilities by at least one order of magnitude [1].

The collaboration envisions a sophisticated experiment capable of reaching the “neutrino floor,” where solar neutrino coherent scattering events become significant, and ultimately deploying improved detectors to achieve even greater sensitivities. In pursuit of these goals, SuperCDMS aspires to contribute groundbreaking insights into the nature of dark matter, advancing the forefront of modern physics and expanding our understanding of the fundamental constituents of the universe [1].

1.2 SuperCDMS Detectors

The SuperCDMS experiment employs a mixture of detectors made of silicon or germanium. There are two detector "styles", called interleaved Z-dependent Ionization and Phonon (iZIP) and High Voltage (HV) detectors [1, 2]. Both of these detectors have similar physical dimensions and fabrication processes and can be composed of either silicon or germanium. The detectors are cylindrical in shape with a radius of 50 mm and a height of 33.3 mm. iZIP detectors distinguish nuclear recoils (NRs) resulting from dark matter interactions, and background sources such as neutron and neutrino interactions with nuclei, as well as electron recoils (ERs) arising from other background sources, by analyzing ionization yield. On the other hand, HV detectors utilize the phonon signal produced by drifting charges to lower the recoil threshold, albeit sacrificing discrimination based on ionization yield [2].

Particles interacting with detector material can knock off electrons and the amount of ionization provides information about the energy of the interacting particle [21]. Phonons are a property of the detector material and are a quantized measure of the crystal lattice's vibrational energy. They are quasi-particles – not particles themselves but are treated as such [14]. When a particle interacts with detector, it can create phonons and the phonons carry information about the energy deposited by the particle [15].

1.2.1 iZIP Detectors

The iZIP detectors, illustrated in Figure 1.1, are equipped with six phonon sensors positioned between inner and outer ionization collection electrodes on both the top and bottom surfaces. The channels on the top and bottom surfaces are rotated by 45° with respect to one another. To create the desired electric fields, voltage biases of ± 3 V (for germanium) or ± 4 V (for silicon) are applied to the top and bottom ionization electrodes, while the phonon sensors are maintained at a near-ground voltage. This configuration generates a vertical electric field within the detector bulk and a strong transverse field near the surface.

By capturing ionization, the iZIP detectors possess the capability to distinguish between electron or gamma-induced electronic recoils (ERs) and neutron, neutrino, or dark matter-induced nuclear recoils (NRs) based on the ionization yield. This yield-based discrimination effectively eliminates ER backgrounds originating from within the detector bulk, provided the recoil energies surpass the threshold at which NRs produce detectable ionization.

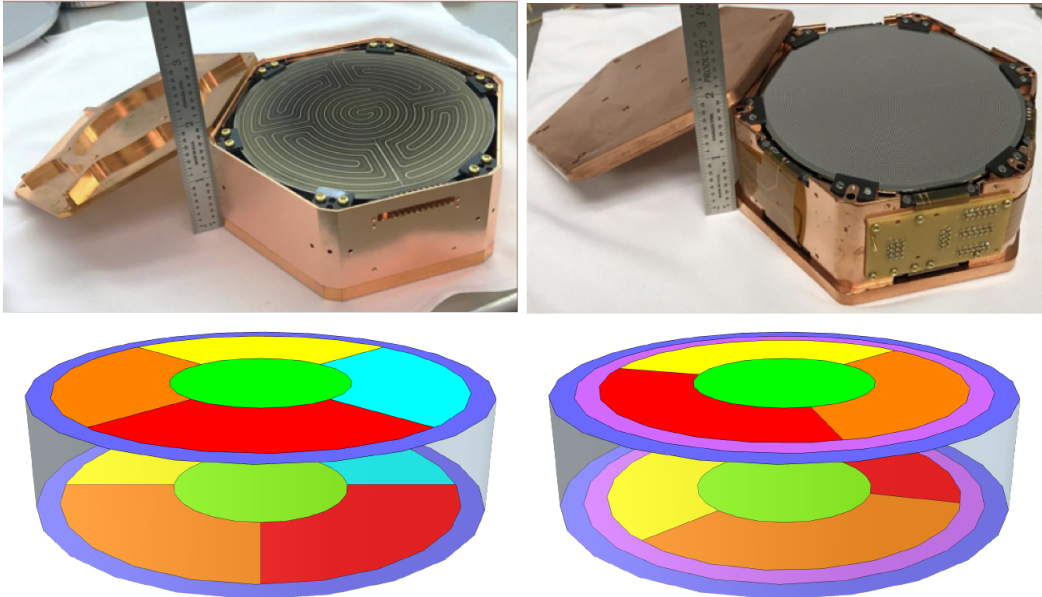


Figure 1.1: The SuperCDMS SNOLAB detectors, from [2]. ”SuperCDMS SNOLAB detectors. (Left) iZIP. (Right) HV. (Top) Prototype detectors in their housings. (Bottom) Channel layout. The iZIP detector has six phonon channels on each side, arranged as an inner core surrounded by four wedge-shaped channels and one outer ring. Each channel contains hundreds of lithographically defined superconducting sensors. An ”outer” ionization channel shares the same area and is interleaved with the outermost phonon ring, and an ”inner” ionization channel is interleaved with the remaining phonon channels. The wedge channels on the bottom surface are rotated by 45° with respect to those on the top. The HV detector has six phonon channels on each side: an inner core surrounded by three wedge-shaped channels and two outer rings designed to reject events near the edge. The wedge channels on the bottom surface are rotated by 60° with respect to those on the top.”

The transverse field, inducing an asymmetry in the ionization signal between the two sides, enables effective rejection of surface backgrounds. This remarkable ability to selectively dismiss a significant portion of background events enables the iZIP detectors to operate with minimal interference from unwanted sources such as electron or gamma-induced ERs [2].

1.2.2 HV Detectors

The HV detectors, depicted in Figure 1.1, incorporate six phonon sensors on each surface, without including ionization sensors. The channels on the top and bottom surfaces are rotated by 60° with respect to one another. These detectors are designed to operate under a bias of approximately 100 V.

This bias enables the utilization of the Neganov-Trofimov-Luke (NTL) effect [11], which amplifies the phonon signal by the amount of energy exerted by the electric field on the charge carriers generated by an interaction as they traverse the detector. This conversion of the ionization signal into phonons reduces the recoil energy threshold due to the substantial phonon signal produced, and the phonon energy threshold remains unaffected by the applied bias (given low ionization leakage). The layout of the phonon-only sensors is optimized to provide positional information based on phonons, which is crucial for distinguishing certain surface backgrounds that might experience diminished NTL amplification [2].

1.2.3 Detector Sensitivity

Figure 1.2 shows the predicted exclusion limits for the SNOLAB SuperCDMS experiment, compared to previous collaborations. The solid lines represent detectors sensitivities from previous experiments, the dashed lines represent the SNOLAB SuperCDMS detectors' sensitivities [1], and the yellow area is the the dark matter discovery limit [13]. The mass-cross-section pairs that are above the exclusion limits are the 90% confidence interval [1], meaning that they are hypotheses that, if one repeated the experiment and the signal did not exist (you only had background), the probability that the background would fluctuate to produce an event yield at least as large as the combined background and signal is less than 10%. Unsuccessful detection of dark matter in these previous experiments excludes the areas above the solid lines, motivating the development of the more sensitive SNOLAB SuperCDMS detectors.

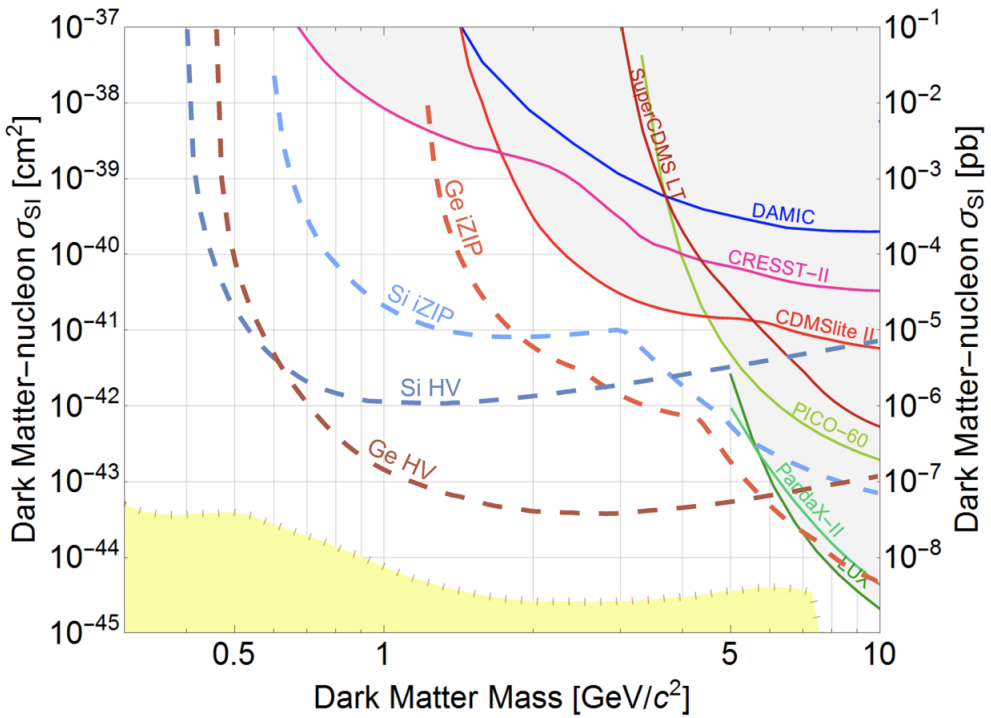


Figure 1.2: Exclusion sensitivity of SNOLAB SuperCDMS detectors using "goal" performance and background levels, from TDR [1]. The vertical axis is the spin-independent dark matter-nucleon cross section, and the horizontal axis is the dark matter particle mass.

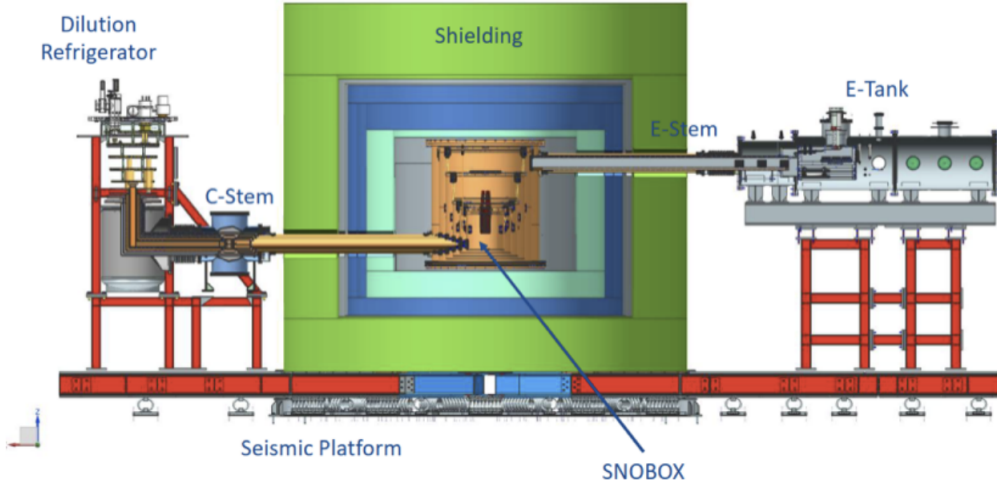


Figure 1.3: SNOLAB SuperCDMS apparatus from [2].

1.3 SuperCDMS Structure

The full experimental apparatus for SNOLAB SuperCDMS is shown in figure 1.3. The detectors will be arranged in towers, with each tower containing six detectors. These towers will be located in the cold region of the experiment, called the SNOBOX, situated 2 km underground in the SNOLAB facility. The SNOBOX consists of six cylindrical copper cans suspended by Kevlar ropes, each linked to a thermal stage of the refrigerator. Surrounding the SNOBOX is a layer of polyethylene for neutron moderation and absorption, followed by a gamma shield made of low-activity lead and an aluminum Rn diffusion barrier. The volume inside the barrier will be purged with nitrogen gas to reduce Rn levels. Additional shielding from cavern neutron flux is provided by polyethylene and water tanks. A mu-metal magnetic shield attenuates Earth's magnetic field. The detectors, housed in copper, are attached to towers mounted on the lid of the lowest-temperature can. These towers also facilitate wiring and cryogenic components for electronics readout, connected via the electronics stem (E-stem) and cryogenics stem (C-stem) to external systems [2].

1.4 Simulation Techniques

The SuperCDMS simulation pipeline consists of several stages [12]. The first stage, SourceSim, simulates particle interactions from the source to the crystal. The output of SourceSim, after post-processing, provides information needed by the Detector Monte-Carlo (DMC), including particle interactions in the crystal, energy deposition,

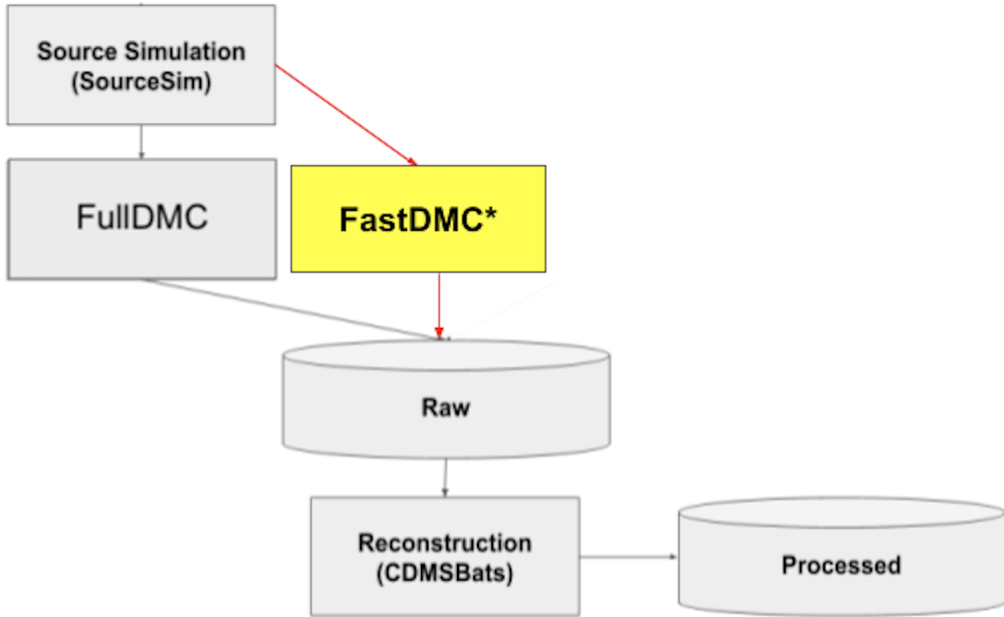


Figure 1.4: SNOLAB SuperCDMS simulation pipeline from [17].

and interaction locations. DMC offers two approaches: FullDMC and FastDMC [17]. FullDMC meticulously simulates the entire detector's physics by tracking individual phonons, electrons, and holes within the crystal lattice. However, its drawback lies in its time-consuming nature, often requiring hundreds of seconds to generate a single event. Conversely, FastDMC estimates detector physics by utilizing a model to compute the energy deposited in each channel based on position, energy, and particle type. Finally, CDMSBats, the event reconstruction software, analyzes simulation events using algorithms similar to those used with real data, retaining truth quantities that can be used to understand the detector response to a given interaction [12]. CDMSBats reconstructs relevant metrics, termed "reduced quantities" (RQs). The simulation pipeline described is shown in figure 1.4.

CDMSBats processes simulated raw data events as though they were real signals, utilizing algorithms such as the optimal filter [12]. This filtering technique requires three inputs: the observed waveform over time, a signal template representing the anticipated shape of real energy depositions, and an estimate of the noise. Subsequently, the algorithm generates three outputs: the most accurate estimate of the signal's amplitude, the time delay of the signal compared to the template, and the χ^2 , a measure of the goodness of fit of the template to the data pulse. Standard simulation techniques allow the option to use either one or two templates, for a one dimensional (1DOF) or two dimensional (2DOF) optimal filter [12].

Letting N be the number of detector channels, CDMSBats creates $Nx1$ (or $Nx2$ if using two templates) RQs each for the phonon amplitudes, time delays, and χ^2 at each detector channel [17]. The simulation pipeline also allows for the tracking of the exact position (x, y, z coordinates) and true energy of the energy depositions [17].

1.5 A Brief Overview of Neural Networks

A feedforward neural network, a fundamental type of artificial neural network, operates as a supervised machine learning model, relying on labelled data for training [22]. Comprising multiple layers, each with numerous nodes or neurons, the network processes input data through these layers to produce an output. At each node, the input is multiplied by a set of weights and then summed, with the result passed through an activation function to generate the output for the next node. This process iterates across all node pairs between consecutive layers until the final layer, which provides the network's predictions [22].

To learn from the data, the network makes predictions and compares them with the actual labels using a loss metric, subsequently adjusting its weights slightly to minimize this loss and improve predictions. Training is typically performed on batches of data, rather than the entire dataset at once, with each complete pass through the dataset termed an epoch. Additionally, a portion of the data, known as the validation set, is reserved for unbiased evaluation of the model's performance during training [22].

When configuring a neural network, key parameters to specify include the number of epochs, the batch size, the architecture (number of hidden layers and neurons per layer), and the choice of activation functions. These parameters play a crucial role in determining the network's ability to learn complex relationships within the data and produce accurate predictions [22]. Frameworks like PyTorch and TensorFlow streamline the training process and computational tasks involved in neural network operations, offering robust automation for model development and optimization.

1.6 Neural Networks in SuperCDMS

A recent report proposes a machine-learning approach to triggering the data acquisition system to record a trace, with the goal of reducing the noise level and the threshold of detection for the SuperCDMS SNOLAB experiment [16]. It suggests upgrading the existing data acquisition system by incorporating a recurrent neural

network. This neural network, to be implemented on the trigger FPGA, aims to improve the accuracy of amplitude estimation and signal-noise discrimination by analyzing filtered traces from individual detector channels. The paper discusses the structure and setup of this neural trigger and predicts that it could reduce the trigger threshold by about 22%. Additionally, it assesses the potential enhancements in key performance measures like efficiency and noise rate using simulations and real noise data.

This study highlights the promise of using neural networks to improve the functionality of triggers in dark matter detection experiments. Thus, such experiments suggest that neural networks can effectively analyze complex signal data from individual detector channels, potentially offering crucial insights to enhance the resolution of SuperCDMS detectors.

Chapter 2

Previous Work & Motivation

Although the signals measured by the detectors inherit information about the position of the source, this information is limited by the number of channels on the detector. Stronger signals at specific channels only imply that the energy deposition may have been in the vicinity of the sensor of that channel. Additionally, it has been noted that the energy resolution of the detectors exhibit some dependence on position. Thus, we were motivated to train and optimize a neural net to measure the location of energy depositions in the detectors, and then use that information to improve the energy resolution.

Aditi Pradeep from University of British Columbia was motivated by the same problem, and studies of the performance of machine learning algorithms for reconstructing the positions of energy depositions.

For her training set, Aditi used a new sophisticated approach to optimal filtering called the NxM optimal filter. The NxM optimal filtering utilizes a statistical method called principal component analysis (PCA) which takes in a dataset of raw phonon signals at N detector channels, and outputs M templates that correlate with the signals in the dataset the most. Using these NxM templates, a new implementation in CDMSBats is able to create NxM RQs correlating to the N detector channels and M principal components. This is advantageous as it provides a larger set of reconstructed data. Note that the current implementation only reconstructs NxM RQs for the phonon amplitudes and not the delays of χ^2 [19].

Principal Component Analysis (PCA) is performed on a set of one-dimensional signal data by first constructing something called a covariance matrix from the data. In the context of PCA for one-dimensional signal data, the covariance matrix quantifies how each signal varies in relation to others, capturing their relationships. Then, eigenvectors and eigenvalues of this covariance matrix are computed. The principal

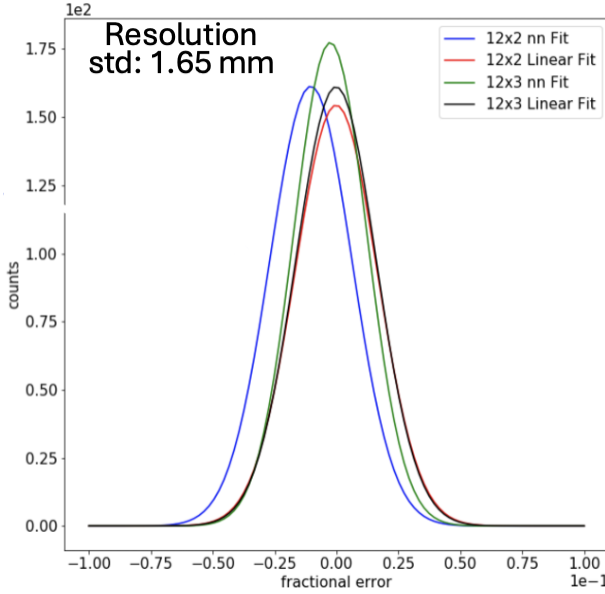


Figure 2.1: Aditi Pradeep’s neural network training results, compared to linear fit, training on NxM phonon amplitudes and predicting X, Y, Z positions from [19].

components, representing the directions of maximum variance in the data, are determined from the eigenvectors associated with the largest eigenvalues. These principal components provide a basis for representing the original signals in a lower-dimensional space [18].

Aditi simulated a dataset of 10,000 detector events of an HV detector, using 12x3 optimal filters (12 channels for an HV detector and 3 principal components selected). She then trained multiple supervised machine learning models using the 12x3 phonon amplitudes as inputs and the X, Y, Z positions as outputs [19]. As can be seen from figure 2.1, her training on a neural network was not very successful, showing results comparable to a simple linear fit. Looking at figure 2.2, we see that Aditi found much more success training a boosted decision tree, another type of supervised machine learning model.

Taking inspiration from Aditi’s work, we were motivated to solve the problem of reconstructing the position and energy of energy depositions in a detector, by testing our methods on various neural networks and datasets.

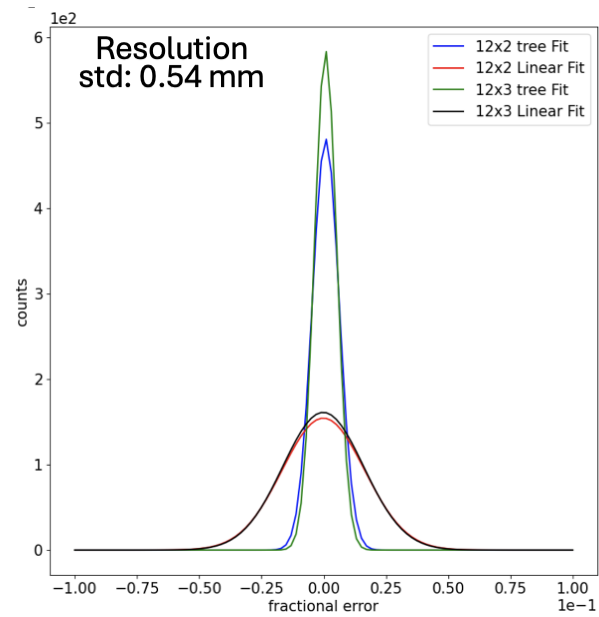


Figure 2.2: Aditi Pradeep's boosted decision tree training results, compared to linear fit, training on NxM phonon amplitudes and predicting X, Y, Z positions from [19].

Chapter 3

Experimental Trials

3.1 Initial Simulations

Before getting into our machine learning, it was important to gain familiarity with the simulation pipeline as well as validate the discrepancies between energy resolution depending on position within the detector volume.

A sample of 1000 events using FullDMC of an iZIP detector was created. Figure 3.1 shows the height and distance from centre of each detector event and identifies low energy efficiency events as events with less than 80% efficiency. This diagram from our simulation validates that there is a lower energy resolution near the detector edges.

3.2 Recreating PCA

Our next step was to validate Aditi's PCA algorithm and choice of principal components. Figure 3.2 shows our raw signals at each channel, where the plot titles are the names of the detector channels, the horizontal axis shows time bins of bin width 1600 ns, and the vertical axis shows the amplitudes measured in Amperes.

Running the PCA algorithm on our dataset, we found principal components for each channel as shown in figure 3.3 for channel PDS1 (axis are the same as figure 3.2). The percent variance for each channel's principal components relative to other principal components is shown in figure 3.4 where the horizontal axis is the principal component number. As can be seen from the figure, the variance significantly decreases after the third principal component, which validates Aditi's choice of using 3 principal components.

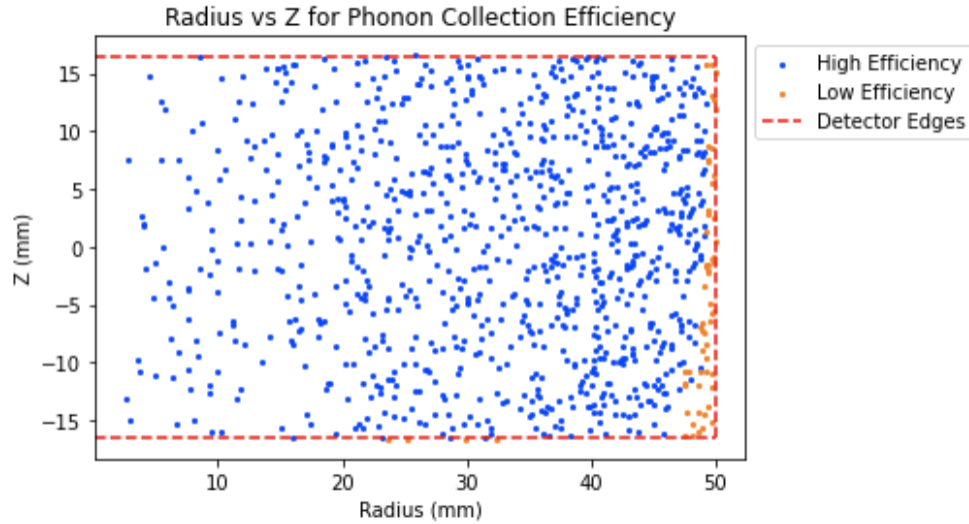


Figure 3.1: Phonon collection efficiency for 1000 samples from a FullDMC simulation of an iZIP detector. Low efficiency is defined as less than 80% collection efficiency.

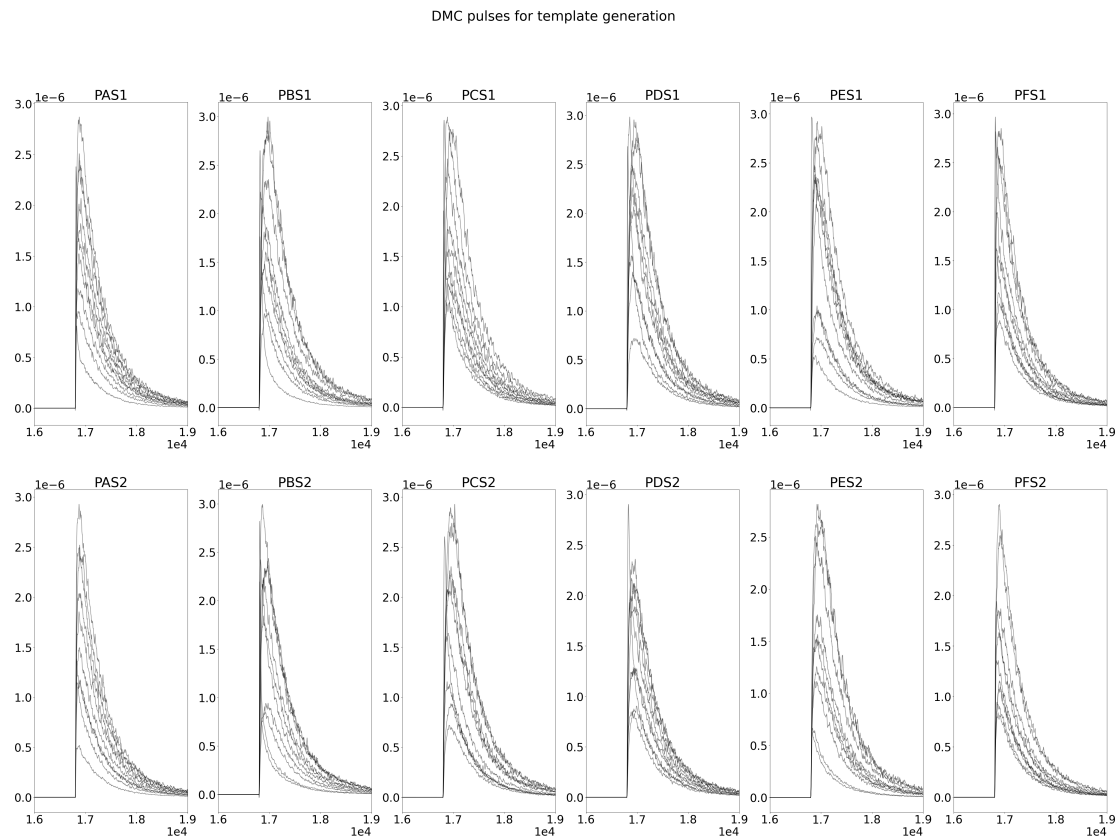


Figure 3.2: Raw phonon pulses at each detector channel from FastDMC of an iZIP detector. The plot titles are the names of the detector channels, the horizontal axis shows time bins of bin width 1600 ns, and the vertical axis shows the amplitudes measured in Amperes.

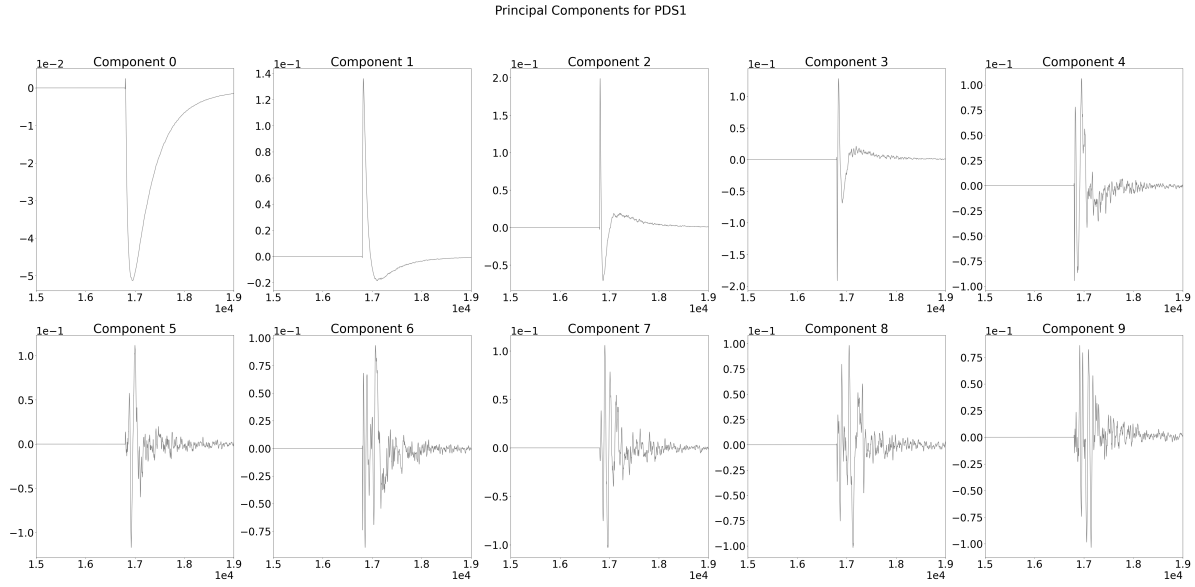


Figure 3.3: Principal components found for detector channel PDS1. The horizontal axis shows time bins of bin width 1600 ns, and the vertical axis shows the amplitudes measured in Amperes.

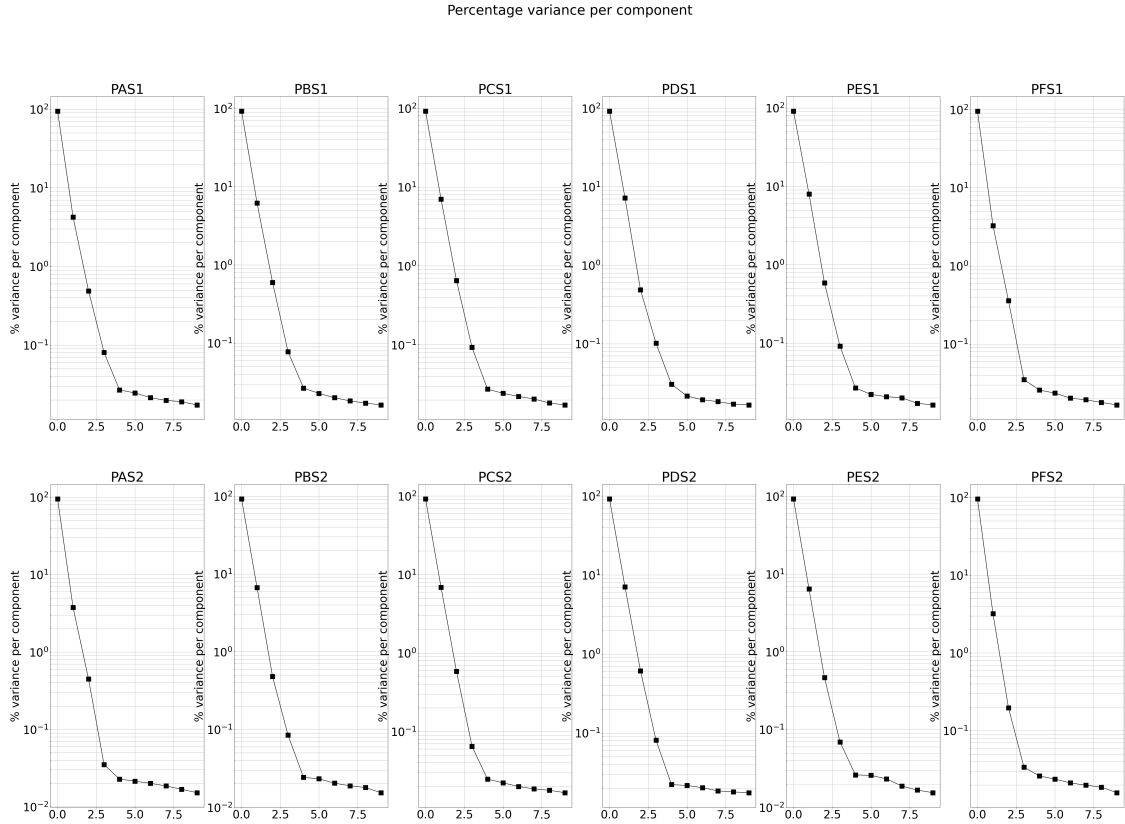


Figure 3.4: Percent variance of principal components found for each detector channel. Horizontal axis is principal component number.

3.3 FullDMC NxM Data & First Trials

3.3.1 Data

Our first trial was using Aditi's original dataset. This was a FullDMC simulated dataset of 10,000 events of an HV detector. This dataset included NxM phonon amplitude RQs for each detector channel, as well as the standard 1DOF RQs for phonon amplitude, phonon delays, and χ^2 . Aditi used 2 principal components so her dataset had 12x4 phonon amplitude RQs to use (since there are 12 detector channels for HV). Aditi's dataset was also monoenergetic, meaning all data points had the same value of true energy.

3.3.2 Feedforward Neural Network Exploration & Optimization

Using the NxM phonon amplitudes as inputs and the X, Y, Z positions as outputs, we started with Aditi's initial neural network which was a simple feedforward neural network architecture implemented using TensorFlow in Python, and only used the first two principal components from her NxM filters, essentially using 12x2 phonon amplitudes as inputs.

The neural network architecture and parameters were tuned using a method called network capacity tuning, in which the number of hidden layers and neurons per layer are tuned to optimize the training and validation loss. After each modification, plots like the one in figure 3.5 were created where the training and validation loss are measured after each epoch of training. These plots allow for the evaluation of the neural network's performance after each modification is made.

3.3.3 Discussion

After tuning the input parameters and architecture, a final neural network was decided on. Our feedforward neural network would use two hidden layers with 64 and 32 neurons, respectively, training with a batch size of 32 for 100 epochs, and using 15% of the dataset for validation.

We also found that Aditi was normalizing each coordinate with respect to the largest in that dimension within the dataset, which could act as morphing the shape of the detector with a limited sized dataset. Thus, we found that our networks learned much faster and with lower loss when normalizing the coordinates with respect to the

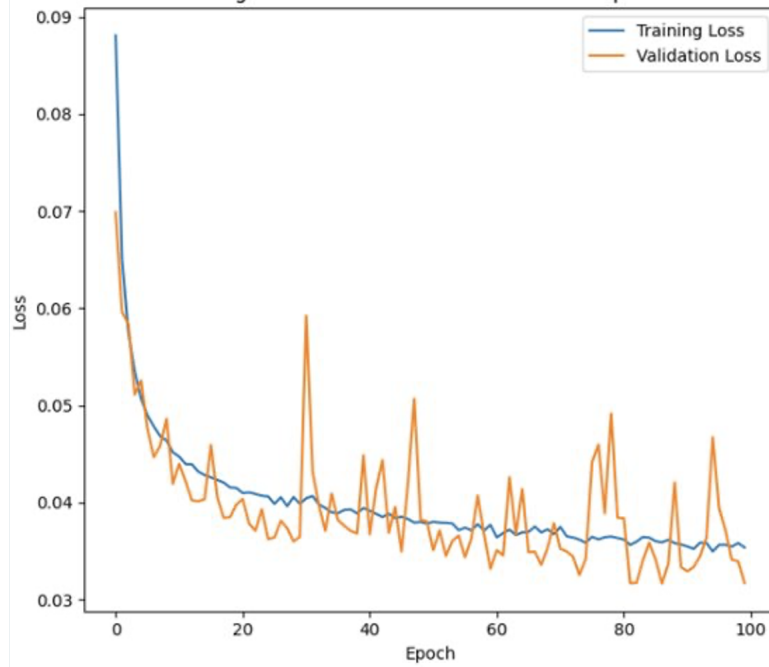


Figure 3.5: Training and validation loss of a neural network after training in Tensor-Flow.

detector's dimensions. That is, the X and Y values were divided by 50 mm, and the Z values were divided by 33.3 mm.

3.4 Exploring 1DOF Data

3.4.1 Motivation for Investigating Signal Delays

Measuring signals at multiple locations in order to determine the origin of the signals is analogous to how satellites for GPS and other LIDAR systems function. These systems determine the origin of their signals by measuring the time delay between the arrival of signals at each receiver [20]. Thus, we were motivated to investigate the neural network's performance after training on the phonon delay RQs.

It is important to note that Aditi's dataset only contained NxM phonon amplitude RQs, but did not have any NxM phonon delay RQs. Thus, in order to test the phonon delay RQs, we must use the 1DOF phonon delay RQs.

Our testing proceeded with four different cases: NxM (12x2) phonon amplitudes as inputs (24 inputs), 1DOF phonon amplitudes as inputs (12 inputs), 1DOF phonon delays as inputs (12 inputs), and both 1DOF phonon amplitudes and delays as inputs (24 inputs).

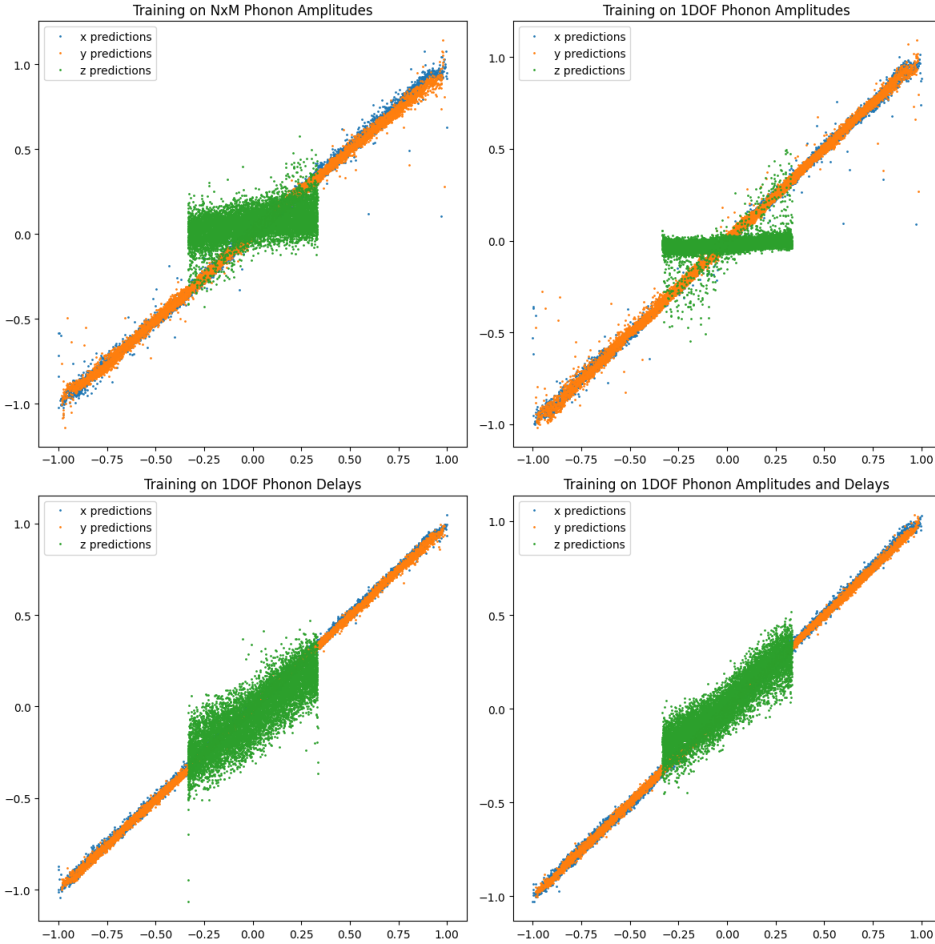


Figure 3.6: Neural network X, Y, Z predictions from training on four different input parameter cases. Horizontal axis is actual (normalized) values, vertical axis is predicted (normalized) values.

3.4.2 Results & Discussion

Figure 3.6 shows the neural network's performance after training on the four different input cases mentioned above, where the horizontal axis is the actual (normalized) coordinates, and the vertical axis is the predicted (normalized) coordinates. As can be seen, all four conditions are able to learn the X and Y positions with comparable performance. From the top two plots it is evident that neither the NxM nor the 1DOF phonon amplitudes are sufficient for learning the Z position, though the NxM network performs slightly better. When training on the 1DOF phonon delays though, it can be seen that the neural network's Z predictions are plotted along the diagonal meaning it is able to predict the Z position better than the latter two cases. Finally, looking at the bottom right plot, it can be seen that the neural network performs best when training on both the phonon amplitudes and the delays.

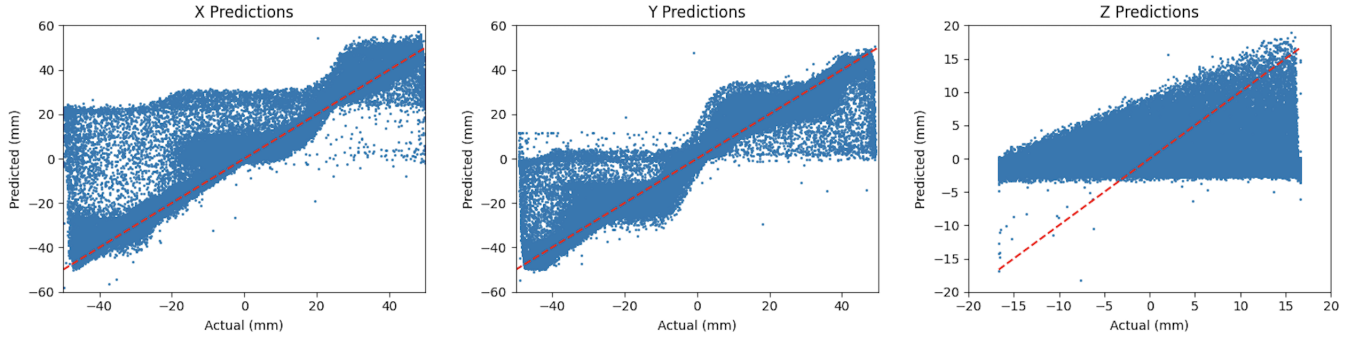


Figure 3.7: X, Y, Z predictions of neural network trained on FastDMC data.

The resolution in the Z-axis, which can be represented by the predicted minus actual Z distribution, shows a standard deviation of 6.90 mm, 8.04 mm, 4.00 mm, and 3.63 mm for the top left, top right, bottom left, and bottom right input cases, respectively. This confirms our observations from the plots in figure 3.6.

Thus, it can be concluded that NxM optimal filtering is not necessary for training a successful model, and that future training can be continued with the 1DOF phonon amplitudes and delays as inputs. This also allows us to generate more training sets without overcomplicating our simulations with the NxM reconstruction.

3.5 Exploring FastDMC Data

3.5.1 Data

In order to train on a larger dataset, Warren Perry from University of Toronto generated a dataset of 100,000 samples from a FastDMC of an HV detector. While Aditi's dataset was monoenergetic, this dataset also included a uniform spectrum of true energy values from 0.05 keV to 2 keV. Since the simulation of phonon delay RQs have not yet been implemented in FastDMC [17], the phonon delay RQs in this dataset all had a value of 0.

We proceeded with training the same neural network architecture from our FullDMC tests, using the phonon amplitude and delay (though all 0) RQs as inputs.

3.5.2 Results & Discussion

Figure 3.7 shows the X, Y, Z predictions made by our model. As can be seen, our model exhibits a strange step pattern in the X and Y predictions, while the Z predictions show a bias towards making predictions above around -5 mm. This

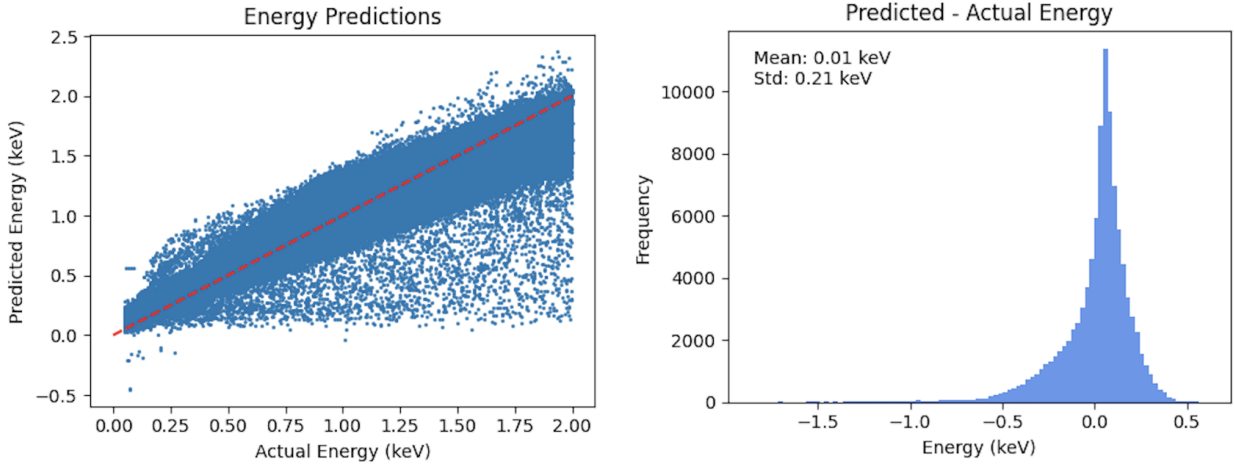


Figure 3.8: Energy predictions from neural network trained on FastDMC data.

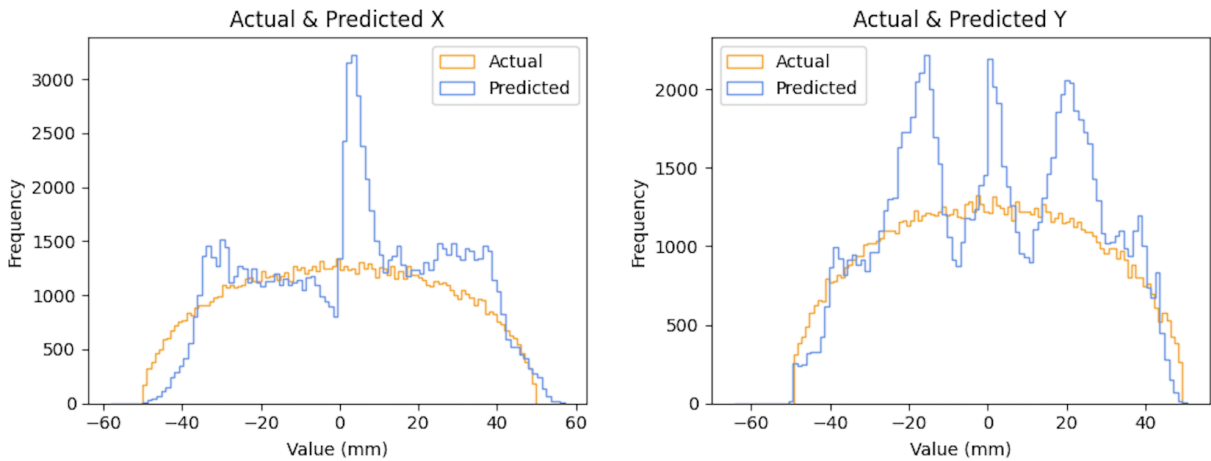


Figure 3.9: 1D histograms of X and Y predictions from neural network trained on FastDMC data compared to actual values.

bias towards (nearly) positive Z predictions is speculative and we are still working to understand them. The energy predictions, shown in figure 3.8 are promising, as the predictions in the scatter plot are mostly along the diagonal, and the resolution (predicted -actual) histogram shows a mean of 0.01 keV and a standard deviation of 0.21 keV.

Taking a closer look at the X and Y predictions and plotting histograms of the predicted values in comparison to the actual values in figure 3.9, we can see that the predictions are concentrated at peaks whereas we expect them to form a semicircular shape due to the geometry of the detector. Plotting these predictions in a 2D histogram in figure 3.10, we see that there is an observable pattern in the prediction peaks; each peak is spaced at 60° around the detector.

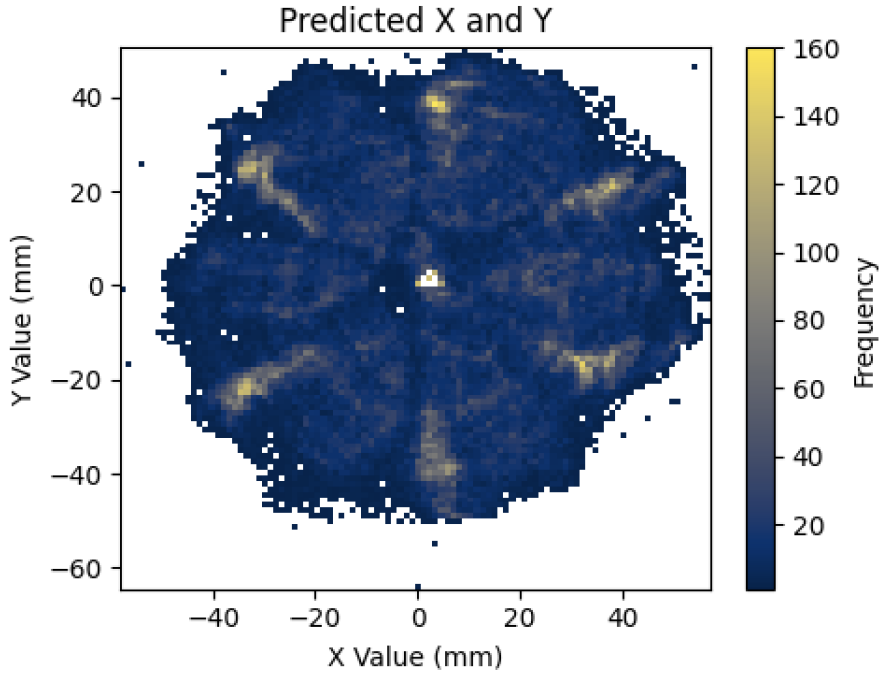


Figure 3.10: 2D histogram of X and Y predictions from neural network trained on FastDMC.

In order to understand these peaks, we must take a closer look at the FastDMC phonon amplitude data. The left plot in figure 3.11 shows the phonon amplitudes measured by one particular detector channel (PCS1), based on the X-Y position of the energy deposition. It can be seen that there is very little energy leakage outside of the channel. Since both sides of the detector are rotated at 60° relative to one another, an inverse of this plot, as shown in the middle plot, would be representative of the opposite side of the detector. Taking this particular pair of detector channels on opposite sides of the detector and overlapping both plots (shown in the very right of figure 3.11, we can get an idea of what the neural network may see in the X-Y plane.

Comparing figure 3.10 and the rightmost plot in figure 3.11, we see that the prediction peaks correspond with the overlapping areas of high phonon amplitudes while the areas between the peaks correspond to the areas of contradicting phonon amplitudes. Thus, the prediction peaks are due to the neural network having high confidence in those areas since all phonon amplitudes at those positions are high. Similarly, the areas with low predictions are due to the neural network observing contradicting phonon amplitudes at the same positions.

Creating similar plots for our FullDMC dataset and predictions, shown in figure

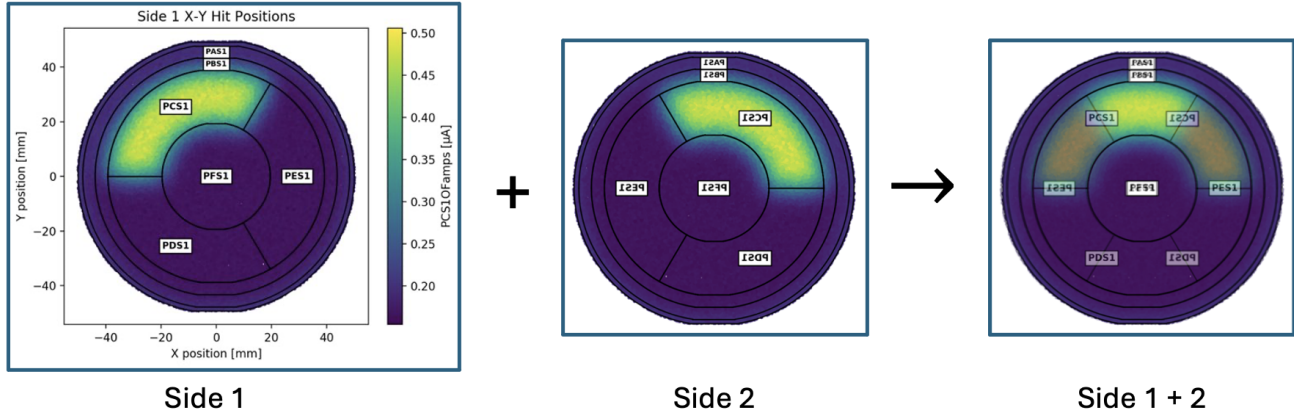


Figure 3.11: Left: Phonon amplitudes measured by detector channel PCS1 from FastDMC dataset, plotted by Warren Perry. Middle: Inverse of left plot to represent opposite detector face. Right: Overlap of middle and left plots to represent neural network's view of X and Y datapoints.

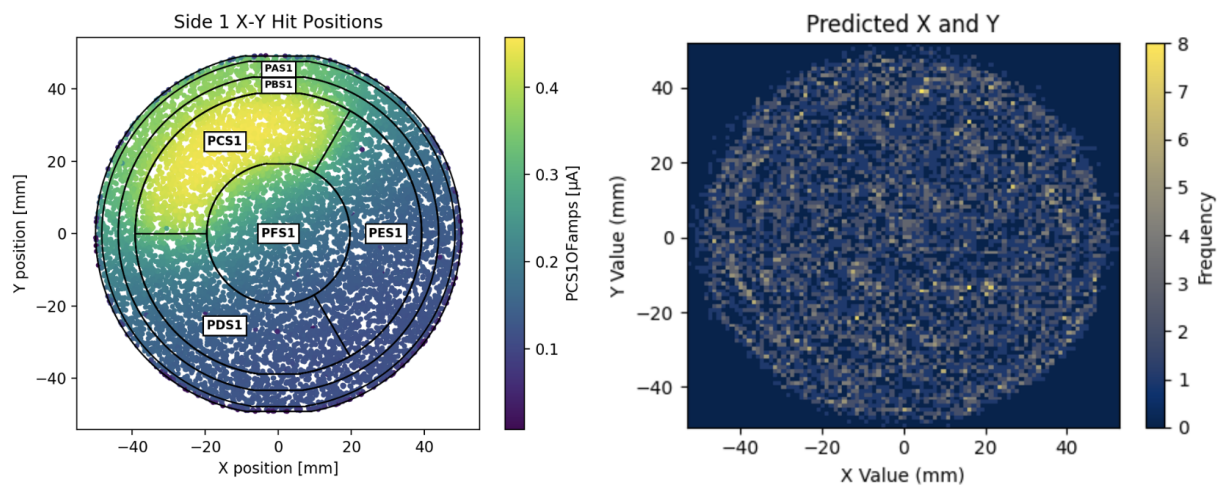


Figure 3.12: Left: Phonon amplitudes measured by detector channel PCS1 from FullDMC dataset, plotted by Warren Perry. Right: 2D histogram of X and Y predictions from neural network trained on FullDMC.

3.12, we see from the left plot that the phonon amplitudes spread more smoothly outside of the selected channel, leading to less distinct areas of high or contradicting phonon amplitudes. Thus, the predictions shown in the right plot are also not concentrated in regions of high predictions.

Comparison of the FullDMC to the FastDMC results show the limitations of the FastDMC simulations, particularly in the energy sharing between different detector channels, and shed some light into possible future improvements to this simulation approach.

Chapter 4

Next Steps

As next steps, it is imperative to delve deeper into the analysis of the FastDMC results, particularly focusing on the Z predictions, which exhibit peculiar patterns requiring further investigation. To gain a comprehensive understanding of the model's performance, it is essential to train a neural network on a non-monochromatic FullDMC dataset, specifically to evaluate its performance in predicting energy values. Given the observed limitations in position predictions from the FastDMC model, it is reasonable to anticipate similar constraints in energy predictions, underscoring the importance of this assessment.

Furthermore, expanding the scope of our experimentation to include simulations of iZIP detectors is crucial. Comparing the outcomes with our existing results derived from HV detector simulations will provide valuable insights into the performance and adaptability of our methodologies across different detector types. This comparative analysis will not only enhance the robustness of our findings but also facilitate a deeper understanding of the underlying principles governing detector behavior.

By undertaking these next steps, we aim to refine and validate our methodologies, paving the way for broader applications and advancements in dark matter detection research.

Chapter 5

Conclusion

Our research has explored the application of neural networks to improve the resolution and energy prediction capabilities of SuperCDMS detectors. Our investigation was motivated by the inherent limitations in current methods, particularly in accurately determining the position and energy of energy depositions within detectors.

Building upon the groundwork laid by Aditi Pradeep's machine learning approach, we embarked on a comprehensive exploration of neural network architectures and optimization techniques. Our experiments involved training neural networks using datasets generated from FullDMC and FastDMC simulations, aiming to enhance the accuracy of energy and position predictions. Despite encountering challenges, such as biases in predictions and limitations in simulation techniques, our research has yielded promising results.

Through rigorous experimentation and analysis, we have demonstrated the potential of neural networks to significantly improve the resolution and energy prediction capabilities of the SNOLAB SuperCDMS detectors. Our findings underscore the importance of continued research in this field, particularly in addressing the challenges posed by biases and limitations in simulation techniques. Additionally, our work highlights the need for further investigation into the performance of neural networks on non-monochromatic datasets and the development of more advanced simulation approaches. Future endeavors will focus on expanding the scope of experimentation to encompass different detector types and simulation scenarios, thereby broadening the applicability and generalizability of the developed techniques.

In conclusion, this report contributes to advancing signal processing methods in the SuperCDMS experiment and lays the foundation for future research aimed at improving the accuracy and efficiency of dark matter detection systems. As we continue to refine and optimize our methods, we move closer to unlocking the mysteries of the

universe's most elusive particles.

Bibliography

- [1] SuperCDMS Collaboration, "SuperCDMS SNOLAB Technical Design Report," Jan. 17, 2018.
- [2] SuperCDMS Collaboration, "A Strategy for Low-Mass Dark Matter Searches with Cryogenic Detectors in the SuperCDMS SNOLAB Facility," Snowmass 2021, Mar. 2022.
- [3] "Dark matter - NASA science," NASA, <https://science.nasa.gov/mission/roman-space-telescope/dark-matter/> (accessed Apr. 22, 2024).
- [4] P. A. R. Ade et al., Planck 2013 results. XVI. Cosmological parameters. *A&A* 571, A16 (2014).
- [5] B. W. Lee and S. Weinberg, Cosmological Lower Bound on Heavy-Neutrino Masses. *Physical Review Letters* 39, 165–168 1977.
- [6] G. Jungman, M. Kamionkowski, and K. Griest, Supersymmetric dark matter. *Physics Reports* 267, 195–373 1996.
- [7] R. Agnese et al., Silicon Detector Dark Matter Results from the Final Exposure of CDMS II. *Physical Review Letters* 111, 251301 December 2013.
- [8] R. Bernabei et al., Dark Matter search. *Rivista del Nuovo Cimento* 26, 1–74 January 2003.
- [9] R. Bernabei et al., First results from DAMA/LIBRA and the combined results with DAMA/NaI. *The European Physical Journal C* 56, 333–355 August 2008.
- [10] R. Agnese et al., CDMSlite: A Search for Low-Mass WIMPs using Voltage-Assisted Calorimetric Ionization Detection in the SuperCDMS Experiment. *Physical Review Letters* 112, 041302 September 2013.

- [11] Luke, P. N. Voltage-assisted calorimetric ionization detector. *J. Appl. Phys.* 64, 6858–6860, DOI: 10.1063/1.341976 (1988).
- [12] J. D. M. Mendoza, “Simulation of the Charge Measurements For the SuperCDMS Soudan Experiment,” PhD Thesis, Texas A&M University, 2020
- [13] F. Ruppin, J. Billard, E. Figueroa-Feliciano, and L. Strigari, Complementarity of dark matter detectors in light of the neutrino background. *Phys. Rev. D*90, 083510 Oct 2014.
- [14] R. C. Ng et al., “Excitation and detection of acoustic phonons in Nanoscale Systems,” *Nanoscale*, vol. 14, no. 37, pp. 13428–13451, 2022. doi:10.1039/d2nr04100f
- [15] Sadoulet, B. [1]; Cabrera, B. [2]; Maris, H. J. [3]; Wolfe, J. P. [4], “Phonon-mediated detection of particles,” Proceedings in PHONON ’89, international conference on phonon physics and 6th international conference on phonon scattering in condensed matter, Heidelberg (Germany, F.R.), 21-25 Aug 1989.
- [16] [1] H. Meyer zu Theenhausen, B. von Krosigk, and J. S. Wilson, “Neural-network-based level-1 trigger upgrade for the supercdms experiment at SNO-LAB,” *Journal of Instrumentation*, vol. 18, no. 06, Jun. 2023. doi:10.1088/1748-0221/18/06/p06012
- [17] Internal SuperCDMS documentation on Confluence, ”Simulations Working Group”
- [18] W. K. Hardle and L. Simar, ”Applied Multivariate Statistical Analysis”. Cham: Springer, 2019.
- [19] Pradeep, Aditi, ”ML applications in the NxM filter”, Internal SuperCDMS Confluence page, (last modified on Mar 30, 2023)
- [20] ”The Global Positioning System for the Geosciences”. Washington, D.C.: National Academy Press, 1997.
- [21] K. Ueda et al., “Roadmap on photonic, electronic and atomic collision physics: I. Light–Matter Interaction,” *Journal of Physics B: Atomic, Molecular and Optical Physics*, vol. 52, no. 17, p. 171001, Aug. 2019. doi:10.1088/1361-6455/ab26d7
- [22] T. L. Fine, Feedforward Neural Network Methodology. New York: Springer, 1999.

